Two-Dimensional Determination of the Cellular Ca^{2+} Binding in Bovine Chromaffin Cells

Mohammad Naraghi,* Thomas H. Müller,# and Erwin Neher*
*Department of Membrane Biophysics, Max-Planck-Institute for Biophysical Chemistry, D-37077 Göttingen, Germany, and
#Physiologisches Institut, Universität Düsseldorf, D-40001 Düsseldorf, Germany

ABSTRACT The spatiotemporal profile of intracellular calcium signals is determined by the flux of calcium ions across different biological membranes as well as by the diffusional mobility of calcium and different calcium buffers in the cell. To arrive at a quantitative understanding of the determinants of these signals, one needs to dissociate the flux contribution from the redistribution and buffering of calcium. Since the cytosol can be heterogeneous with respect to its calcium buffering property, it is essential to assess this property in a spatially resolved manner. In this paper we report on two different methods to estimate the cellular calcium binding of bovine adrenal chromaffin cells. In the first method, we use voltage-dependent calcium channels as a source to generate calcium gradients in the cytosol. Using imaging techniques, we monitor the dissipation of these gradients to estimate local apparent calcium diffusion coefficients and, from these, local calcium binding ratios. This approach requires a very high signal-to-noise ratio of the calcium measurement and can be used when well-defined calcium gradients can be generated throughout the cell. In the second method, we overcome these problems by using calcium-loaded DM-nitrophen as a light-dependent calcium source to homogeneously and quantitatively release calcium in the cytosol. By measuring $[Ca^{2+}]$ directly before and after the photorelease process and knowing the total amount of calcium being released photolytically, we get an estimate of the fraction of calcium ions which does not appear as free calcium and hence must be bound to either the indicator dye or the endogenous calcium buffer. This finally results in a two-dimensional map of the distribution of the immobile endogenous calcium buffer. We did not observe significant variations of the cellular calcium binding at a spatial resolution of ~ 2 μm. Furthermore, the calcium binding is not reduced by increasing the resting $[Ca^{2+}]$ to levels as high as 1.1 μM. This is indicative of a low calcium affinity of the corresponding buffers and is in agreement with a recent report on the affinity of these buffers (Xu, T., M. Naraghi, H. Kang, and E. Neher. 1997. *Biophys. J.* 73:532–545). In contrast to the homogeneous distribution of the calcium buffers, the apparant calcium diffusion coefficient did show inhomogeneities, which can be attributed to restricted diffusion at the nuclear envelope and to rim effects at the cell membrane.

INTRODUCTION

A detailed understanding of calcium (Ca^{2+}) dynamics in excitable cells requires a quantification of different sources and sinks for Ca^{2+} ions. A generic scheme of Ca^{2+} signaling can be viewed as consisting of the following components (Clapham, 1995): influx of Ca^{2+} from some extracytosolic compartment into the cytosol, diffusion of Ca^{2+} as well as binding of Ca^{2+} to different buffers (which can be endogenously present in the cell or added exogenously by means of patch pipettes), and uptake into internal Ca^{2+} stores or extrusion across the plasma membrane. The influx of Ca^{2+} across the plasma membrane is well-characterized by means of patch-clamp recordings whereas the diffusional spread of Ca^{2+} ions while binding to different cellular buffers, the so-called "buffered diffusion problem," has received much less attention. Once the impact of these buffers as Ca^{2+} sinks is understood, one can quantitatively study the remaining determinants of Ca^{2+} signals, which are given by fluxes across different biological membranes, such as membranes of the endoplasmic reticulum or mitochondria. It is the study of the buffered Ca^{2+} diffusion in single bovine chromaffin cells that this paper is dedicated to.

Several imaging studies have revealed intracellular gradients of the free Ca^{2+} concentration ($[Ca^{2+}]$) in different cell types (Williams et al., 1985; O'Sullivan et al., 1989; Kasai and Augustine, 1990; Huser et al., 1996). In bovine adrenal chromaffin cells, $[Ca^{2+}]$ gradients were seen to dissipate within a few hundred milliseconds (Neher and Augustine, 1992) and this time course was prolonged if the concentration of the Ca^{2+} indicator was increased. Since the dye competes with endogenous buffers in binding Ca^{2+}, the dye-dependent changes in the recovery time course of the $[Ca^{2+}]$ signal were used to estimate the average Ca^{2+} binding ratio of the cytoplasm of chromaffin cells under whole-cell recording conditions. Later, using the perforated patch method, Zhou and Neher (1993) were also able to distinguish between the capacity of mobile and immobile endogenous Ca^{2+} buffers in chromaffin cells, but again as a cellular average. These studies have prompted a series of investigations that aimed at determining the cytosolic buffering power of various cell types (for a review see Neher, 1995).

Ca^{2+} signaling inherently involves three problem dimensions, namely time, space, and amplitude, and the range of

Received for publication 29 October 1997 and in final form 13 February 1998.

Address reprint requests to Dr. Mohammad Naraghi, Dept. of Membrane Biophysics, Max Planck Institute for Biophysical Chemistry, Am Fassberg 11, D-37077 Göttingen, Germany. Tel.: 49-551-201-1675; Fax: 49-551-201-1688; E-mail: mnaragh@gwdg.de.

0006-3495/98/10/1635/13 $2.00

action of a Ca^{2+} signal heavily depends on spatial buffering properties of the cytoplasm (Allbritton et al., 1992; Wagner and Keizer, 1994). This in turn raises the question of whether a given cell can be regarded as spatially homogeneous with respect to its buffering power or whether it constitutes a highly differentiated medium for spatial Ca^{2+} signals: an intriguing possibility, especially for polarized cells that use Ca^{2+} as a fast second messenger. Nevertheless, there is no quantitative report on spatially resolved measurements of Ca^{2+} binding properties of cells up to this day. Here, we attempt to establish methods to assess the distribution of Ca^{2+} binding sites in a cell under the whole-cell mode of the patch-clamp technique. We show that the effective spatial resolution is dictated by the acquisition rate of the imaging system and out-of-focus effects due to light diffraction. In the specific case of cultured adrenal chromaffin cells, we do not see signs of heterogeneity of fixed Ca^{2+} buffer distribution on a micrometer spatial scale, which, of course, does not exclude gradients of Ca^{2+} buffers on a submicrometer scale.

MATERIALS AND METHODS

Cell preparation and solutions

Chromaffin cells in primary culture from bovine adrenal glands were prepared and cultured as described previously (Smith and Neher, 1997). Cells were used for experiments 1–4 days after plating in culture dishes. The standard external bath solution for experiments contained (in mM): 140 NaCl, 2.8 KCl, 5 $CaCl_2$, 1 $MgCl_2$, 20 HEPES, and 2 mg/ml glucose (pH 7.2, 310 mOsm). The internal solutions were based on a 2× concentrated buffer containing (in mM): 290 cesium glutamate, 40 HEPES, and 12 NaCl (pH 7.2). After adding appropriate amounts of indicator dye or DM-nitrophen (DMN) or $CaCl_2$, this solution was diluted twofold to give the final internal solution with an osmolarity of 300–320 mOsm and pH 7.20.

DMN was purchased from Calbiochem (La Jolla, CA); Fura-2, Bis-Fura-2, and BAPTA were purchased from Molecular Probes (Eugene, OR). All other chemicals were from Sigma (St. Louis, MO).

Combining patch-clamp, digital Ca^{2+} imaging, and flash-photolysis of DMN

Our experiments required patching the chromaffin cells, loading them with the fluorescent dye, and activating the voltage-dependent Ca^{2+} channels by short depolarizing pulses as well as imaging the $[Ca^{2+}]$ distribution. In some experiments it was also necessary to photorelease Ca^{2+} from Ca^{2+}-loaded DMN by short pulses of UV light. The apparatus to achieve this goal is schematically depicted in Fig. 1. It is centered around an inverted Zeiss microscope, Axiovert 135 TV. Two light sources are coupled into the epiillumination port of the microscope: a UV flash lamp (Rapp Optoelektronik, Hamburg, Germany) and a polychromatic light source (T.I.L.L. Photonics, Gräfeling, Germany), which is based on a xenon lamp. It chooses the appropriate wavelength by positioning a grid on a galvanometric scanner. The grid position is set by analog signals from a control unit, which receives commands from a master PC. The same PC is also used to trigger the flash lamp and the depolarizing voltage pulses of the patch-clamp amplifier (EPC-9, HEKA Electronic, Lambrecht, Germany) via a Macintosh Quadra 950 computer. The flash light passes a UG11 filter and an appropriate neutral density filter and is finally directed via a 50%/50% beam splitter to the back pupil of a 40× water immersion Zeiss objective (NA = 1.2, C-APOCHROMAT). The 50% transmission of the same beam splitter is also used to feed the fluorescence excitation light of the polychromatic source into the objective. By directing a fraction (8%) of the light to a photodiode, we also monitored the light intensities by sampling the output of a photodiode amplifier using the master PC. In addition, the objective was mounted on a piezoelectric element (Pifoc, Physik Instrumente, Germany), driven by a PC-controlled unit, which enabled us to acquire images at different focal planes with a precision of 10 nm, if needed.

For the acquisition of the fluorescent images, a water-cooled frame-transfer CCD camera was used. The images were stored with a dynamic range of 12 bits on the PC and later transferred to a SPARC-10 (SUN Microsystems, Cupertino, CA) UNIX workstation for analysis. Finally, in the diffusion experiments, it was crucial to maximize the signal-to-noise ratio (SNR) of the Ca^{2+} images. We achieved this goal by increasing the supply current of the xenon lamp and, thus, the excitation light intensity. A voltage between 1 and 2 V, provided to a controlled power supply, was converted to a current (with a gain of 1 V/5 A), which was added to the normal supply current (5.4 A) for the xenon lamp. This pulsing of the power supply enabled us to increase the excitation intensity by a factor of 3 for a few hundred milliseconds, which gave rise to a corresponding increase in the fluorescent counts during the pulsing. However, it was not possible to maintain the high excitation intensity for >500 ms because the lamp would otherwise become unstable (as was monitored by the photodiode).

Mathematical model for diffusion and method for calculating local diffusion coefficients

The idea in the first set of experiments was to observe the diffusive dissipation of $[Ca^{2+}]$ gradients and then to extract local apparent Ca^{2+} diffusion coefficients from a fit of the theoretically expected $[Ca^{2+}]$ time course to the experimentally observed one. Consequently, we need a mathematical model of the expected $[Ca^{2+}]$ time course in the presence of different mobile or immobile calcium buffers. Intuitively, the presence of an immobile endogenous Ca^{2+} buffer would slow down the diffusion and, thus, show up as a reduced apparent Ca^{2+} diffusion coefficient. A mobile Ca^{2+} buffer, however, would shift the apparent Ca^{2+} diffusion coefficient toward the mobile buffer's diffusion coefficient as an increasing fraction of Ca^{2+} is being carried by the buffer. A formalization of this idea was given by Wagner and Keizer (1994) within the framework of the rapid buffer approximation (rba) to the buffered diffusion problem. In the rba, one assumes that all buffers, whether mobile or immobile, have such fast Ca^{2+} binding kinetics that they are in chemical equilibrium with local $[Ca^{2+}]$ at every instant of time and at every point in the cell. In other words, the time scale for dissipation of the $[Ca^{2+}]$ gradients is supposed to be much slower than the time scale on which the Ca^{2+} binding reactions approach chemical equilibrium. If this is true, the dynamics of $[Ca^{2+}]$ can be described by a single nonlinear partial differential equation

$$\frac{\partial[\mathrm{Ca}^{2+}]}{\partial t} = \frac{1}{1 + \sum_i \kappa_i} \nabla\left\{\left(D_{\mathrm{Ca}} + \sum_i D_i \kappa_i\right) \cdot \nabla[\mathrm{Ca}^{2+}]\right\}, \qquad (1)$$

where D_i and κ_i are the diffusion coefficient and the Ca^{2+} binding ratio of the ith buffer B_i. Note that the binding ratios $\kappa_i = ([B_i]_T K_i/(K_i + [Ca^{2+}])^2)$ are nonlinear functions of $[Ca^{2+}]$ and the buffer's dissociation constant K_i. If, however, the affinity of the buffers is low, i.e., $[Ca^{2+}] \ll K_i$, then $\kappa_i = [B_i]_T/K_i$ is independent of $[Ca^{2+}]$. Otherwise, in case of small $[Ca^{2+}]$ excursions, κ_i can be regarded as independent of $[Ca^{2+}]$ as well. Then, assuming that the free and Ca^{2+}-bound form of mobile buffers have the same diffusion coefficient, Eq. 1 can be simplified to

$$\frac{\partial[\mathrm{Ca}^{2+}]}{\partial t} = \frac{D_{\mathrm{Ca}} + \sum_i D_i \kappa_i}{1 + \sum_i \kappa_i} \Delta[\mathrm{Ca}^{2+}], \qquad (2)$$

which is the classical diffusion equation with an apparent Ca^{2+} diffusion coefficient given by $D_{app} = (D_{Ca} + \Sigma_i D_i \kappa_i)/(1 + \Sigma_i \kappa_i)$. In whole-cell

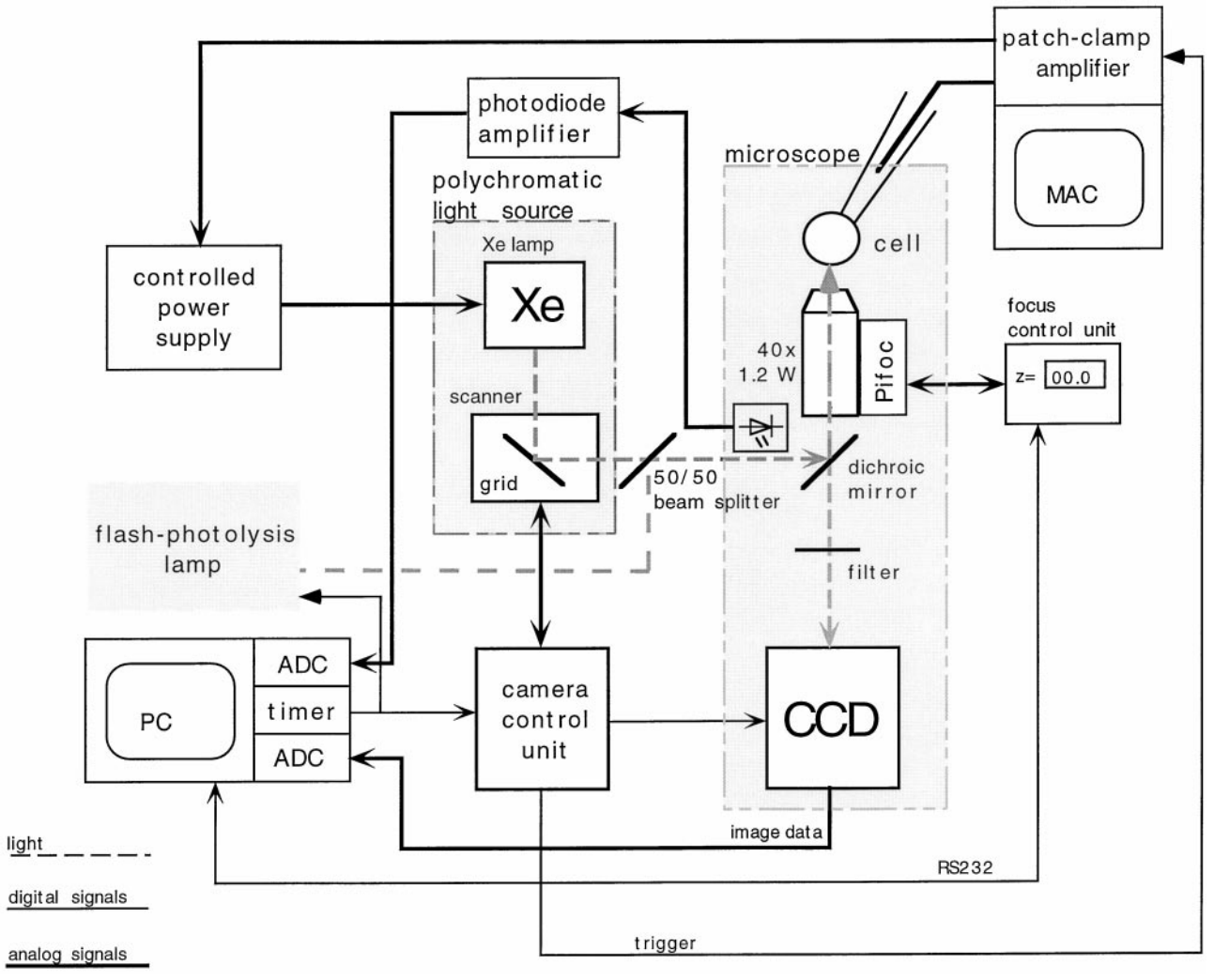

FIGURE 1 Scheme of the apparatus for Ca^{2+} imaging and flash photolysis. The setup is built around an Axiovert 135 TV. Two light sources are coupled into the microscope using a 50%/50% beam splitter: steady-state light (from a xenon lamp) for fluorescence excitation and flash light for photolysis. The power supply of the xenon lamp was pulsed for a few hundred milliseconds to increase the excitation power. The light intensity and the flash time course are monitored by a fast photodiode, which receives ~8% of the total light power. All the equipment is controlled and synchronized by a "master PC," which also reads in the image data from a 12 bit water-cooled frame transfer CCD camera.

recordings, any endogenous mobile Ca^{2+} buffer washes out within minutes (see Zhou and Neher, 1993). Consequently, one is left with the fluorescent Ca^{2+} indicator, which is a mobile buffer, and immobile endogenous Ca^{2+} buffers, which we lump together into one species. This results in

$$D_{app} = \frac{D_{Ca} + \kappa_{ind} D_{ind}}{1 + \kappa_{ind} + \kappa_{endo}} \tag{3}$$

with κ_{endo} representing the binding ratio of the immobile endogenous buffer, the quantity we want to determine. Note that a heterogeneous distribution of the fixed buffer shows up in a heterogeneous distribution of D_{app}, as expected intuitively. The problem can now be restated as follows: by using $[Ca^{2+}]$ imaging, we observe the solution to the system (Eq. 2) and ask for its structural parameters, namely the spatial distribution of D_{app}. This problem is mathematically referred to as a so-called "inverse problem"; the "direct problem" being the calculation of the $[Ca^{2+}]$ time course from a knowledge of all system parameters, which is the classical domain of simulation studies.

As a first method, one is tempted to calculate D_{app} as the ratio $(\partial[Ca^{2+}]/\partial t)/(\Delta[Ca^{2+}])$. This, however, corresponds to multiple high-pass filtering operations on $[Ca^{2+}]$ images and leads to an explosion of the noise level, which makes any meaningful interpretation of the results impossible. Consequently, we decided to take another approach for estimating D_{app} based on nonlinear regularization theory (Tarantola, 1987; Louis, 1989). Let us denote by D_{theo} an arbitrary distribution of apparent Ca^{2+} diffusion coefficients in the cell. Assume that at time zero we have a $[Ca^{2+}]$ distribution, which we denote by c_{init}. Δt ms later, diffusive spread of Ca^{2+} will cause a $[Ca^{2+}]$ profile c_{theo}, which of course depends on D_{theo}. We write this dependence as $c_{theo} = c(D_{theo})$. We can now compare the theoretically expected Ca^{2+} distribution, c_{theo}, with the experimentally observed one, c_{obs}, and adjust the diffusion coefficients in such a way that c_{theo} best matches c_{obs}. This is the regularization approach, which results in D_{app} as a solution to the multidimensional optimization problem of minimizing the error functional $f(D_{theo})$:

$$\underset{D_{theo}}{Minimum}\, f(D_{theo}) \equiv \underset{D_{theo}}{Minimum}(\|c(D_{theo}) - c_{obs}\|^2 + \epsilon\|D_{theo}\|^2) \tag{4}$$

In other words, we look for a D_{app} distribution that optimally reproduces the observed spatiotemporal $[Ca^{2+}]$ profile (the first term in the above sum) and simultaneously has some degree of smoothness (the second term in the sum). The trade-off between these two aspects is controlled by the regularization parameter ϵ, which in general is selected empirically and causes the solution to the above problem to be unique. The next issue is then how to solve the minimization problem given in Eq. 4. For this end, we used many methods under which the Gauss-Newton and the conjugate-gradient method (Press et al., 1992) were the fastest algorithms. Here, we outline the conjugate-gradient method:

1. Choose initial distribution $D^{(0)}_{theo}$ (spatially homogeneous), set $i = 0$;
2. Compute $d^{(0)} = r^{(0)} = -(\partial f(D^{(0)}_{theo})/\partial D_{theo})$. This calculation of the derivatives of the error functional f with respect to the parameters D_{theo} involves solving a parabolic system of partial differential equations, which we performed using the Cranck-Nicholson algorithm. The dimension of this system is identical to the number of pixels in the cell;
3. Find $\gamma^{(i)}$ that minimizes $f(D^{(i)}_{theo} + \gamma^{(i)}d^{(i)})$ using a line search algorithm;
4. Set $D^{(i+1)}_{theo} = D^{(i)}_{theo} + \gamma^{(i)}d^{(i)}$;
5. Compute $r^{(i+1)} = -(\partial f(D^{(i+1)}_{theo}/\partial D_{theo})$ [exactly like (2)];
6. Set $\beta^{(i+1)} = (\|r^{(i+1)}\|^2/\|r^{(i)}\|^2)$, $d^{(i+1)} = r^{(i+1)} + \beta^{(i+1)}d^{(i)}$;
7. Increment i to $i + 1$ and go to step (3).

The regularization parameter ϵ was determined empirically by simulating the diffusion process and adding noise (before backcalculating the diffusion coefficients) to achieve the same SNR as in the $[Ca^{2+}]$ measurement. Then we applied the inverse algorithm with different values for ϵ and compared the estimated diffusion coefficients with the ones we used for the simulation of the diffusion process. This procedure identified a range of applicable parameters, the values used were between 0.001 and 0.005.

Estimation of endogenous Ca^{2+} binding ratios with photolysis of DMN

Some inherent problems, which are detailed in the Discussion part of this paper, prompted us to reattack the estimation problem of the binding ratios with a different approach. The rationale here was the following: if we manage to photorelease Ca^{2+} from DMN quantitatively (Zucker, 1993) and rapidly compared with the mean diffusional equilibration time of Ca^{2+} gradients, the Ca^{2+} ions can either bind to some buffers or appear as free Ca^{2+} only at the pixel where they have been released. The more buffer one has at a given pixel, the smaller the increase in $[Ca^{2+}]$ upon photorelease will be. In other words, the increase in $[Ca^{2+}]$ is a measure of the total Ca^{2+} binding ratio of the cell at each and every pixel, as long as no significant spread of Ca^{2+} ions to neighboring pixels happens. The total Ca^{2+} binding ratio at every pixel is in turn the sum of binding ratios of exogenous and endogenous buffers. This consideration results in the following pixelwise identity:

$$\Delta[Ca^{2+}]_{total} = (1 + \kappa_{ind} + \kappa_{DMN} + \kappa_{endo}) \cdot \Delta[Ca^{2+}], \quad (5)$$

where $\Delta[Ca^{2+}]$ is the difference in $[Ca^{2+}]$ before and after the flash. Thus, we need to know the total amount of Ca^{2+} released by a flash (from calibration measurements), $\Delta[Ca^{2+}]_{total}$, the binding ratios κ_{DMN} and κ_{ind}, and measure the difference between free Ca^{2+} concentration after and before flash, $\Delta[Ca^{2+}]$, to calculate κ_{endo}. If the exogenous buffers are homogeneously distributed in the cell (by virtue of their mobility) and the Ca^{2+} release pattern is also homogeneous in the cell, every spatial heterogeneity in $\Delta[Ca^{2+}]$ can only result from a heterogeneous distribution of the fixed endogenous buffer. This again gives us quantitative information about binding ratios and their distribution without expensive and noise-sensitive diffusion measurements.

RESULTS

Diffusion experiments

As indicated above, our goal was to study the relaxation of depolarization-induced $[Ca^{2+}]$ gradients in the cytosol of chromaffin cells. For this end, we recorded in whole-cell mode with pipette solutions, which contained 100 μM Fura-2 but no ATP to exclude any further exogenous Ca^{2+} buffer. The choice of the Fura-2 concentration was a compromise between the following opposing constraints. a) One would like to aim at as small Fura-2 concentrations as possible, since the indicator is only a reporter of the Ca^{2+} signal and should minimally perturb the system. Increasing dye concentration would eventually lead to an exogenous binding ratio much bigger than the endogenous one. Then, the endogenous buffer will not affect the Ca^{2+} signal by modulating the apparent Ca^{2+} diffusion constant and, hence, will not be visible in the measurement. b) Alternatively, the SNR of the Ca^{2+} measurement is a critical factor for the inverse estimation procedures, which we outlined above. Since the SNR is itself determined by the number of photoelectrons generated at each pixel of the camera chip during acquisition of an image, the aim is to catch as many photons as possible per pixel and image integration time. But what parameters do we have at our disposal to increase the number of photons? These are threefold: higher dye concentrations, higher excitation intensities, and longer integration times per image. Observation of the gradient dissipation necessitates high acquisition rates; hence, we cannot afford to increase image integration time. Consequently, we chose to use 100 μM Fura-2, which gives rise to a binding ratio of 45 at $[Ca^{2+}] = 500$ nM, the maximal acquisition rate of 40 Hz for single wavelength measurements, and to increase the excitation intensity for 200–300 ms by a factor of 2–3 within the acquisition time, by pulsing the power supply as outlined in Materials and Methods.

Fig. 2 shows two such series of $[Ca^{2+}]$ images from different cells with 25 ms integration per frame. In *A* and *B* the lowermost images were taken at rest with a holding potential of -60 mV. During the next frame, the cell was depolarized to 0 mV while all other images were taken again at -60 mV. In both cases, one can clearly identify initial $[Ca^{2+}]$ rises underneath the plasma membrane, whereas the pattern of spatial spread of these Ca^{2+} signals is quite distinct. In (*A*), the nucleus is located in the lower-right quarter of the cell (as identified in transmission images) while Ca^{2+} entry mostly occurs within a rim of the membrane on the opposite site of the cell. The incoming Ca^{2+} gives rise to cytosolic $[Ca^{2+}]$ gradients, which spread toward the nucleus within 100 ms. The nucleus seems to constitute a diffusion barrier since, even after 200 ms, there is a marked difference between the cytosolic and nuclear Ca^{2+} concentration. This is a type of cell which is not accessible to our inverse methodology for estimating apparent Ca^{2+} diffusion coefficients, because major parts of the cell only have very flat Ca^{2+} gradients and, consequently,

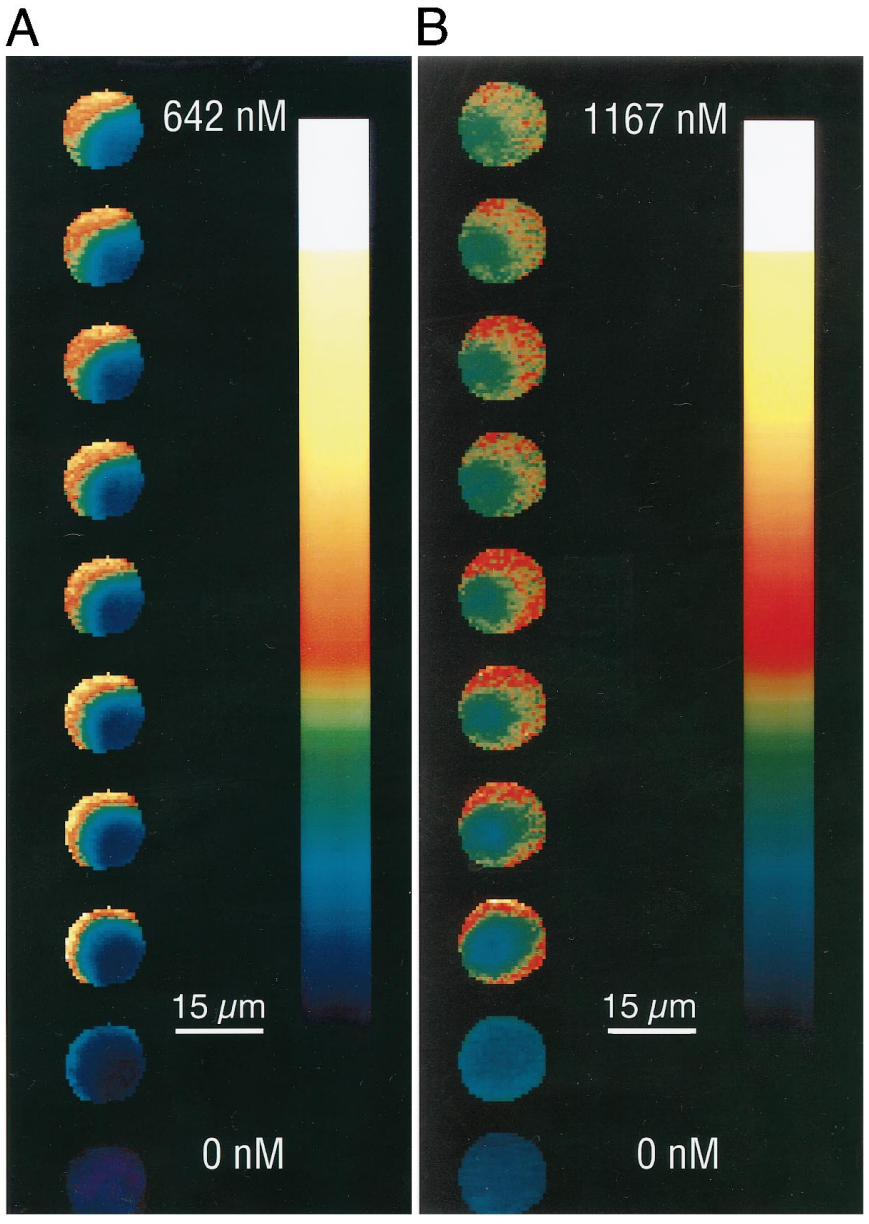

FIGURE 2 Pseudocolored images of depolarization-induced $[Ca^{2+}]$ gradients in adrenal chromaffin cells. Depicted are two series of $[Ca^{2+}]$ images (from two different cells) acquired at 40 Hz with 25 ms exposure time per frame. In (*A*) and (*B*), the image at the bottom is acquired at a resting membrane potential of −60 mV. During the next frame, the cell was depolarized to 0 mV while all other images are again at $V_m = -60$ mV. In (*A*) the nucleus is located at the lower right quarter of the cell (visible in transmission images, not shown here) while the Ca^{2+} influx mostly happens at the opposite quarter. Furthermore, the nucleus seems to constitute a pronounced diffusion barrier for Ca^{2+}. The Ca^{2+} influx in (*B*) occurs across a major part of the plasma membrane, and consequently a Ca^{2+} wave spreads toward the center of the cell.

hardly any information can be obtained. In (*B*), Ca^{2+} appears to spread into the cytosol in a radial fashion (in the first two or three images after the depolarizing pulse) while we still see signs of hindered diffusion around the nucleus. Nevertheless, when attempting to estimate Ca^{2+} diffusion coefficients in two-dimensional (2-D) images, we have to cope with some inherent problems.

1) The measured fluorescence is influenced by out-of-focus light, which causes blurring. Likewise, Ca^{2+} diffuses into and out of the focal plane (which should be rather called a focal slice) while $[Ca^{2+}]$ is measured at only one slice. Unfortunately, we are not able to reconstruct the spatiotemporal $[Ca^{2+}]$ profile in response to a depolarizing pulse in 3-D because of the acquisition time needed for a frame; and we cannot repeat the same experiment at different focal planes since channel statistics and current rundown imply that the $[Ca^{2+}]$ distribution is never guaranteed to be the same by repeating the same pulse many times at different focal planes.

2) A cross-section of a typical chromaffin cell is represented by ~1000 pixels in 2-D with a physical pixel size of ~500 nm × 500 nm. Thus, from the relaxation of the gradients, one needs to estimate 1000 unknowns, namely the diffusion coefficients at each pixel. This is algorithmically a very expensive task and requires high-end computing power in conjunction with a very high SNR.

We could derive a partial solution to these problems by using the observation that in some cells, the Ca^{2+} gradients appeared to be approximately radial. To qualify a cell for this radial approach, it had to fulfill two conditions: the integral of $[Ca^{2+}]$ had to be constant between consecutive images (to exclude release or uptake processes), and the $[Ca^{2+}]$-profiles along neighboring lines through the center of the cell had to be almost identical (note that within the

image acquisition time, the Ca^{2+} signal spreads ~1–2 μm, as discussed later). This reduced the problem to estimating the diffusion coefficients along a line. Two line profiles, 25 ms apart, together with the theoretically expected profile using the estimated diffusion coefficients, are plotted in the top panel of Fig. 3. The bottom panel shows the corresponding distribution of the diffusion coefficients where one can clearly discern spatial heterogeneities of Ca^{2+} mobility. The Ca^{2+} diffusivity is lowest under the plasma membrane. Moving further into the cell, one identifies two local minima of D_{app}. Comparison with transmission images reveals that these minima are located right at the positions where the nuclear membrane is, while the high D_{app} values correspond to the nucleoplasm. This would translate into the following pattern for the immobile endogenous buffer distribution: higher levels close to plasma or nuclear membrane and low expression levels within the nucleus.

But there are alternative ways to explain these results. The nuclear membrane can constitute a diffusion barrier and, thus, its effect can show up as a reduced Ca^{2+} diffusion coefficient. This in combination with optical blurring of the fluorescence can then give rise to the broad minima of D_{app}, which we observe in Fig. 3, without an underlying increase in the immobile Ca^{2+} binding ratio. Likewise, at the boundary of the cell, restricted diffusion and blurring effects can cause reduced D_{app} values. We could not exclude any of these possibilities, since we cannot observe the $[Ca^{2+}]$ time course in 3-D, and both hindered diffusion and high immobile binding ratios will show up as low D_{app} within our framework. To distinguish between these alternative interpretations, we used flash photolysis as another means to estimate κ_{endo}.

Photolysis experiments

In this set of experiments, it was crucial to measure the $[Ca^{2+}]$ distribution immediately after photolytic release of

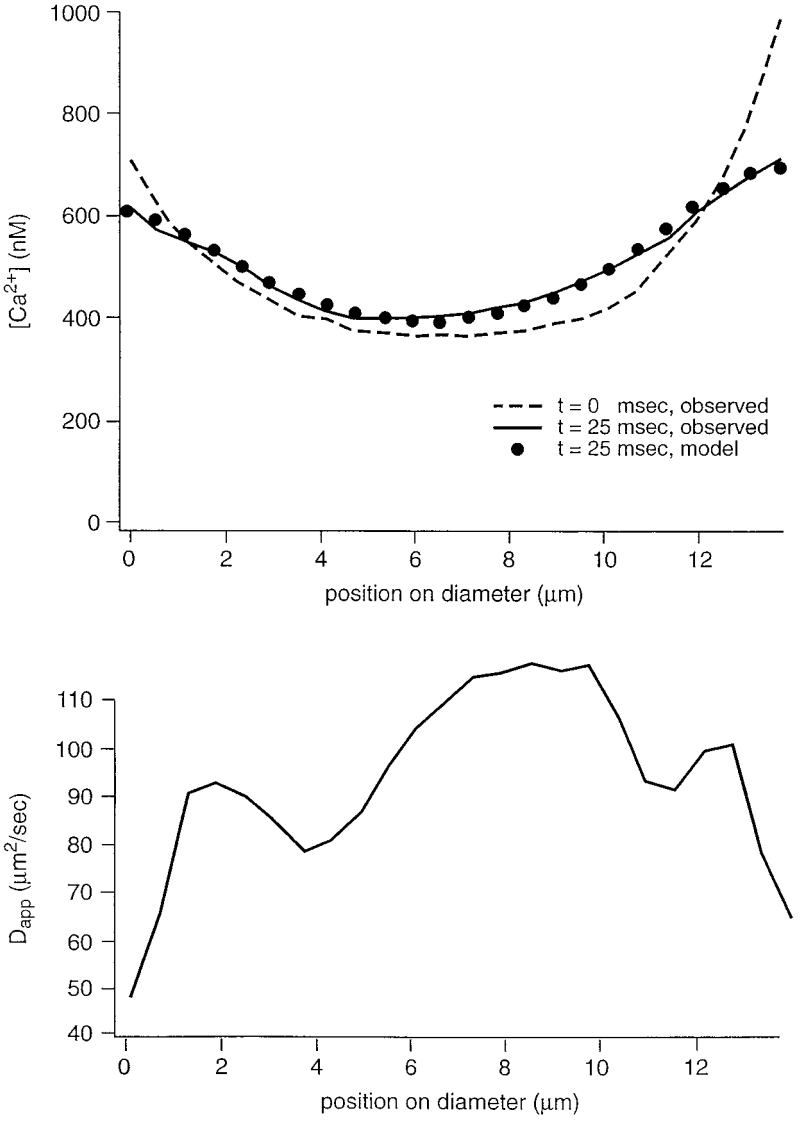

FIGURE 3 Relaxation of $[Ca^{2+}]$ gradients and estimation of the apparent Ca^{2+} diffusion coefficients along a line through the center of the cell. The top panel shows two consecutive $[Ca^{2+}]$ line profiles, which are taken 25 ms apart. Superimposed is also the theoretically expected $[Ca^{2+}]$ profile (*filled circles*), which one would see as the solution to the diffusion equation 25 ms after the observed initial $[Ca^{2+}]$ distribution ($t = 0$ ms, observed), if the distribution of the apparent diffusion coefficients, D_{app}, is as given in the bottom panel. The regularized estimates for the diffusion coefficients show local minima at the boundary of the cell, i.e., close to the plasma membrane, as well as close to the nuclear membrane.

Ca^{2+}. If the release pattern is homogeneous and the exogenous buffers are uniformly distributed in the cell, every heterogeneity in $[Ca^{2+}]$ can only result from a nonhomogeneous pattern of fixed endogenous buffer distribution.

As a reporter dye, we decided to use Bis-Fura-2 for several reasons. It has the same Ca^{2+} binding group as Fura-2 but two fluorophores (of Fura-2 type) are attached via linkers to the chelating group. This should give rise to a higher fluorescence yield and, thus, enable us to use smaller dye concentrations to achieve a desired SNR. The top panel in Fig. 4 shows the absorption spectra of 50 μM Bis-Fura-2 at different $[Ca^{2+}]$ levels. Comparison with Fura-2 data (not shown here) reveals that the absorption is indeed twice that of Fura-2. A plot of the fraction of Ca^{2+}-bound dye over $[Ca^{2+}]$ in the bottom panel shows that the dissociation constant of Bis-Fura-2 for Ca^{2+} is 500 nM, i.e., two-fold higher than Fura-2. This implies that, at a given concentration, its binding ratio is smaller than that of the high-affinity Fura-2 and, hence, its distortion of Ca^{2+} signals less pronounced. Another relevant issue for our measurements is the binding kinetics of the dye. It determines two factors: 1) conventional $[Ca^{2+}]$ measurements with fluorescent indicators use the equilibrium form of the law of mass action to deduce $[Ca^{2+}]$ from fluorescence data, using some modification of the Grynkiewicz et al. (1985) formalism (see the Appendix in our case). Consequently, we must allow the dye to get in chemical equilibrium with free Ca^{2+}. This imposes a lower limit on the minimal integration time per frame. The kinetics of Bis-Fura-2 was investigated in a recent report (Naraghi, 1997), which resulted in an on-rate of 5.5×10^8 M s^{-1} and an off-rate of 260 s^{-1}. Thus, the equilibration time constant is <4 ms. This matches our integration time of 25 ms/frame.

2) The flash lamp generates short pulses of UV light with a total duration of 2–3 ms. Within this time, Ca^{2+} is released into the cell and is subject to binding and unbinding to free DMN, Bis-Fura-2, and endogenous buffers. Dependent on the Ca^{2+} binding kinetics of these buffers, there might be a transient Ca^{2+} spike, which is more pronounced if the Ca^{2+} release rate is higher than the binding rates of the different buffers (Heinemann et al., 1994). The Grynkiewicz formalism is not applicable during this transient

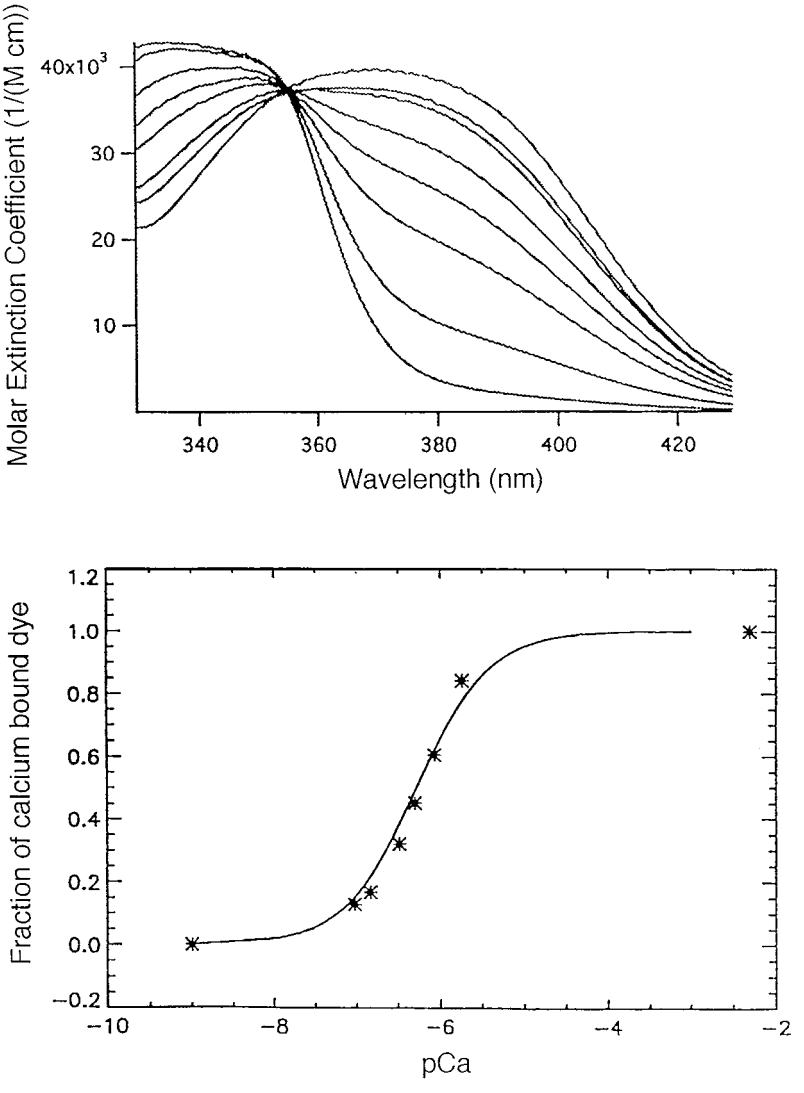

FIGURE 4 Absorption spectra of 50 μM Bis-Fura-2 at different $[Ca^{2+}]$ levels and the titration curve for Ca^{2+} binding to Bis-Fura-2. The top panel shows the molar extinction coefficients of Bis-Fura-2 at different Ca^{2+} concentrations, ranging from <1 nM (*top curve* at 380 nm) to >5 mM (*bottom curve* at 380 nm), demonstrating that it undergoes a shift of its absorption upon Ca^{2+} binding just like Fura-2. From these data the ratio of the Ca^{2+}-bound Bis-Fura-2 over total Bis-Fura-2 was calculated and plotted as a function of $[Ca^{2+}]$ in the bottom panel. Fitting these data with a binding curve (*superimposed line*) reveals a K_D value of 500 nM. (Note: The $[Ca^{2+}]$ for the curves in the top panel can be seen as abscissa values in the bottom panel.)

spike if the dye is not in equilibrium with Ca^{2+}. These considerations imply that we need to estimate the amplitude and duration of such a probable spike. With this information, one can decide on the appropriate timing for the $[Ca^{2+}]$ measurement after the UV flash. Xu et al. (1997) have measured the in vivo Ca^{2+} binding kinetics of DMN and Fura-2 in chromaffin cells. They found the kinetics of Fura-2 to be little affected by the cytosolic medium, which gives us the justification to assume the same for Bis-Fura-2. Furthermore, they also showed that the chromaffin cells contain 4 mM of an immobile endogenous buffer with a K_D of 100 μM and an on-rate of 1.0×10^8 M s^{-1}. By using this well-defined set of parameters and the rates of release of Ca^{2+} from DMN (Ellis-Davies et al., 1996), we performed a 4th order Runge-Kutta simulation of the temporal evolution of the concentrations in response to a flash of light. The time course of the flash as a perturbation (which shifts the system from one equilibrium state to another) was sampled by a fast photodiode and used in the simulation. Fig. 5 shows the outcome of such a simulation for a typical experimental condition. Clearly, there is a transient Ca^{2+} spike of a few hundred nM amplitude within the first 3–4 ms after the flash. Nevertheless, it is not seen by the indicator, which is acting as a low-pass filter and achieves equilibrium within 5 ms. The fast endogenous buffer with its low affinity, however, does follow the $[Ca^{2+}]$ time course faithfully. The conclusion from these simulations is if we start the post-flash $[Ca^{2+}]$ measurement 3 ms after the onset of the flash, we can be sure that there is no significant contamination of the recorded fluorescence by nonequilibrium conditions. This is exactly what we did.

The next important issue was to check whether the photolysis is spatially homogeneous. First, using a mirror in the object plane, we imaged the intensity distribution of the widefield excitation pattern as well as that of the flash light in the focal plane. Both appeared to overlap quite well and were homogeneous, but this could not exclude the possibility that the Ca^{2+} source, i.e., CaDMN, was still compartmentalized. If this was the case, one would see spatial gradients of $[Ca^{2+}]$ after the flash, which were the result of compartmentalized CaDMN rather than different endogenous buffer concentrations. To exclude this possibility, we designed a control experiment to prove that the Ca^{2+} source strength was uniform throughout the cell. This was a simple "buffer overload" experiment: with 2 mM of Bis-Fura-2 and 1–2 mM fully loaded DMN in the pipette, we outcompeted the endogenous buffers in binding Ca^{2+}. Thus, a homogeneous $[Ca^{2+}]$ distribution after the flash could only be the result of a homogeneous source and sink, i.e., CaDMN and indicator distribution. Fig. 6 demonstrates the outcome of such a control experiment. We have plotted the fluorescence ratios as a function of pixel number before and after the flash. Clearly, the ratios are homogeneous. This means that we can now proceed with our experiments designed to assess the endogenous buffer distribution.

Here, we used the same timing protocol for photolysis and imaging as above but with an internal solution, which

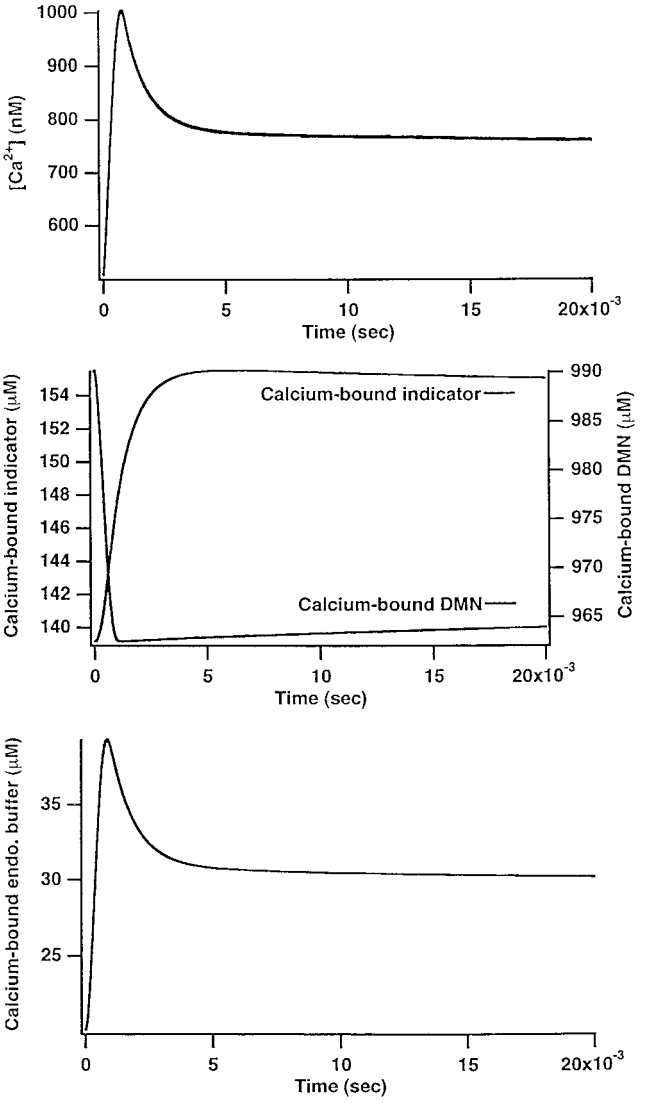

FIGURE 5 Time course of the concentrations of Ca^{2+} and Ca^{2+}-bound buffers after a flash. The measured time course of the flash is used in this simulation to perturb the kinetic system from one equilibrium state to another one. Here, we assume to have 1 mM DMN, 0.2 mM Bis-Fura-2, and 4 mM of an endogenous buffer with a K_D of 100 μM according to Xu et al. (1997). The kinetic parameters for the exogenous buffers are taken from Naraghi (1997) or Ellis-Davies et al. (1996). Clearly, there is a transient overshoot of $[Ca^{2+}]$, which lasts ~2 ms and is seen by the endogenous buffer by virtue of its fast kinetics. Nevertheless, this is invisible to the dye (acting as a low-pass filter of the $[Ca^{2+}]$ time course), which attains equilibrium after 3 ms. Thus, we can start the $[Ca^{2+}]$ measurement 3 ms after the onset of the flash without any transient contaminations.

contained 1 mM fully loaded DMN, 200 μM Bis-Fura-2, and different amounts of $CaCl_2$ such that $[Ca^{2+}]$ was adjusted to values between 500 and 1100 nM. Note that under these conditions the binding ratio of the dye is between 100 and 39, i.e., of the same order of magnitude as the endogenous buffer according to Xu et al. (1997), and between 20 and 4 for DMN. The fraction of DMN, which we wanted to cleave upon a flash, i.e., the photolysis efficiency, was adjusted to 2–7%. This choice was dictated by many con-

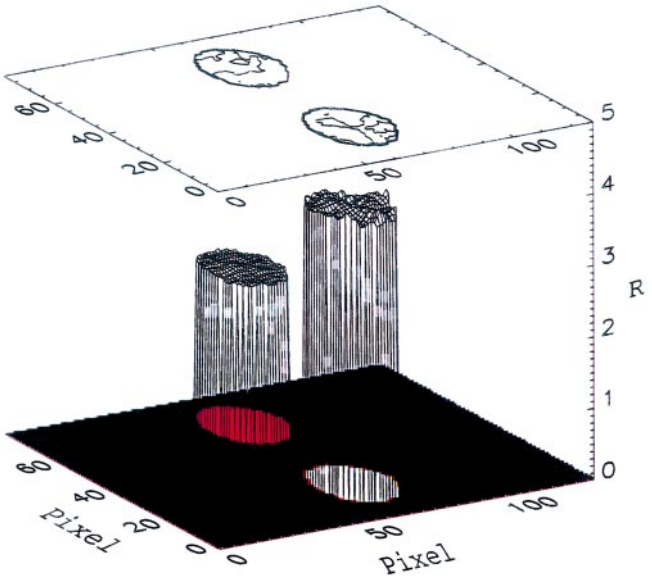

FIGURE 6 Homogeneity of the photolysis pattern. A cell was loaded with 2 mM Bis-Fura-2 (to overcome the endogenous buffers) and 1 mM DMN. Depicted are the fluorescence ratios (R) before and after a flash. We see that the photolysis efficiency is spatially uniform since the same is true for the ratio distribution.

siderations: a) calibration parameters of the dye are not changed for small flash intensities, b) the identity in Eq. 5 is only valid for small values of $\Delta[Ca^{2+}]$ since it is based on the linear approximation

$$\kappa_X = \frac{\partial[CaX]}{\partial[Ca^{2+}]} \approx \frac{\Delta[CaX]}{\Delta[Ca^{2+}]},$$

and c) only small increments in $[Ca^{2+}]$ guarantee that the binding ratios of the dye and the DMN are not changed significantly upon flash. This is not an issue for the endogenous buffer since it is expected to have a K_D around 100 μM. Fig. 7 (*top*) shows the result of such an experiment where we have plotted the $[Ca^{2+}]$ distribution before and after flashes. Clear postflash gradients of $[Ca^{2+}]$ are not discernible. The bottom panel shows the calculated distribution of the endogenous binding ratio according to Eq. 5. The values for κ_{endo} scatter between 30 and 55. Similar experiments at different $[Ca^{2+}]$ levels with 17 cells never revealed a pronounced heterogeneity in the distribution of κ_{endo}; and in accordance with the low affinity of the endogenous buffer, we did not see any signs of a decrease in the average cellular κ_{endo} value by increasing $[Ca^{2+}]$ up to 1.1 μM. These results must be contrasted with the results of the diffusion experiments, which is what we do in the next section.

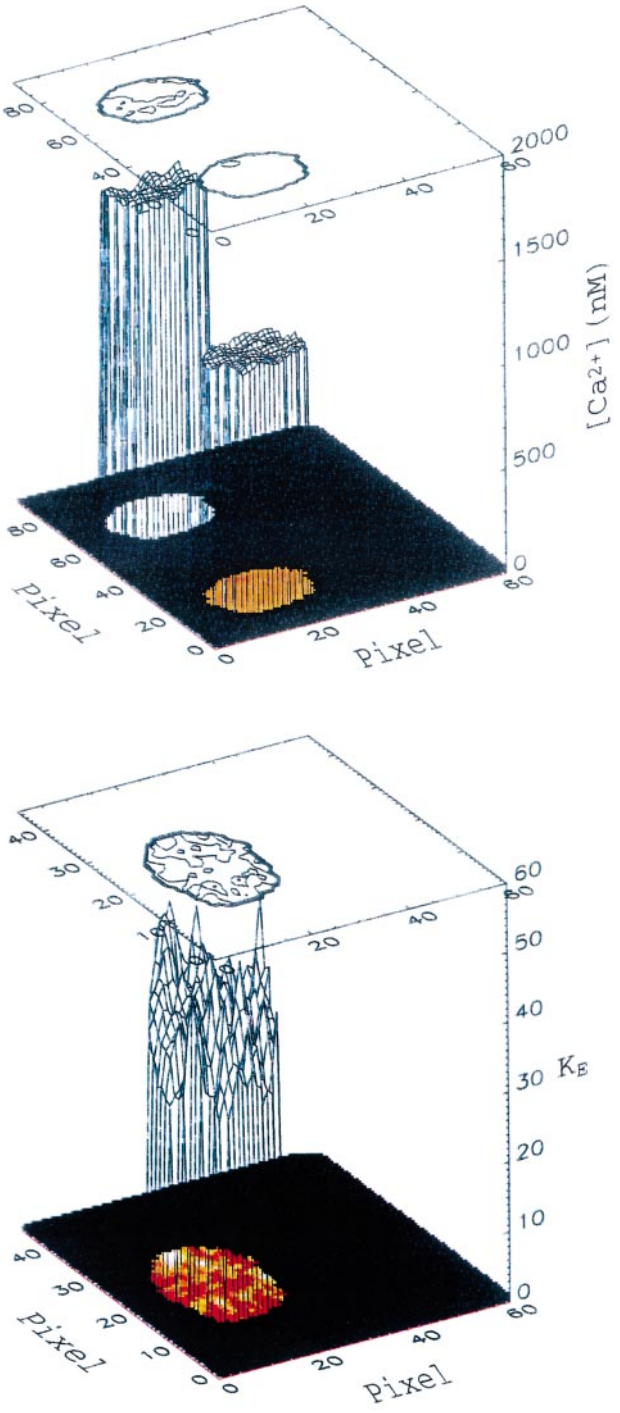

FIGURE 7 Distribution of pre and postflash $[Ca^{2+}]$ as well as the calculated endogenous binding ratios. The top panel shows the $[Ca^{2+}]$ profile before and in response to a UV flash. From these two images, the distribution of κ_{endo} was calculated according to Eq. 11 and plotted in the bottom panel.

DISCUSSION

In light of the increasing evidence for functional but not necessarily morphological Ca^{2+} compartments (Chad and Eckert, 1984; Imredy and Yue, 1992; Llinas et al., 1995), it has become clear that Ca^{2+} signaling must rely heavily on a balanced, local, and quantitative interplay between different sources and sinks of Ca^{2+}. The generic objective of a cell, using Ca^{2+} as a highly controlled and ubiquitous second messenger, is to achieve a specific pattern of $[Ca^{2+}]$

distribution in response to a specific stimulus, which fulfills three conditions: a) the strength of the $[Ca^{2+}]$ signal must be within a well-defined amplitude window, which is matched to the affinity of the desired target of the Ca^{2+} signal; b) the duration of the $[Ca^{2+}]$ signal must be within a well-defined time window to account for the activation kinetics of the desired target, which in turn is governed by the binding and unbinding kinetics of Ca^{2+} to the sensor responsible for triggering the signaling cascade; and c) the transient $[Ca^{2+}]$ elevation must happen at the location where the corresponding Ca^{2+} sensor is located, and maybe only there.

These are conditions imposed on the source. Analogously, requirements can be formulated for the sinks, which can be quite distinct and heterogeneous in nature: they can be energy-consuming pumps and exchangers, intracellular organelles, or single chelating molecules. It is well known that the first two categories of sinks are often equipped with rather slow activation kinetics (in the range of hundreds of milliseconds and longer; see Neher and Augustine, 1992, or Markram and Sakmann, 1994) while the temporal window on which the buffers operate is dictated by their Ca^{2+} binding rate. Recent studies on Ca^{2+} binding kinetics of the endogenous buffer in adrenal chromaffin cells (Xu et al., 1997) show that they can constitute Ca^{2+} sinks, which act in a submillisecond time domain. Within a millisecond or so, Ca^{2+} is expected to diffuse <1 μm (Allbritton et al., 1992). Thus, the fast buffer effects are local effects. Consequently, in polarized neuroendocrine cells or in neurons, the notions of fast and local Ca^{2+} signals must be regarded as synonymous. And if this is true, one can expect to have a differential Ca^{2+} buffering power at different locations of the cell with different functional fingerprints. But how can we assess this possible differential buffer distribution?

An answer to this question can only be given operationally from a functional, i.e., physiologist's, point of view. Since we do not know how many different molecular species are involved in fast Ca^{2+} buffering and have no direct evidence for their chemical identity, we must look for a common property that defines their action regardless of their identity. In other words, this property must reflect the buffers' action in reducing and localizing the Ca^{2+} signal. Following Mathias et al. (1990) and Neher and Augustine (1992), this important property of a cellular buffer is the extent to which it is capable of binding Ca^{2+} ions at a given free Ca^{2+} concentration. That is, what is the buffers' effect on relating a change in total Ca^{2+} to a change in free Ca^{2+}? This question readily suggests studying the so-called "Ca^{2+} binding ratio (κ_B)" of a buffer B, defined as $\kappa_B = \partial[CaB]/\partial[Ca^{2+}]$. Several studies have investigated the cellular binding ratio by lumping together the combined action of all cellular buffers in terms of a hypothetical Ca^{2+} binding species (for review see Neher, 1995).

Zhou and Neher (1993) were able to dissect two different types of endogenous Ca^{2+} buffers in bovine adrenal chromaffin cells: an immobile species (because it was detectable after prolonged periods of whole-cell recording without significant washout) with a binding ratio of 40, and a slowly mobile species (because, after transition to whole-cell mode, it washed out slowly) with a binding ratio of 10. Furthermore, from the time course of the decline of this binding ratio after breaking into the cell, they could estimate the corresponding buffer's molecular weight to be $\sim$10,000. Unexpectedly, they did not find any signs of highly mobile endogenous Ca^{2+} buffers, such as nucleotides, but these numbers are all cellular averages and do not reflect any spatial differentiation of the cell with respect to the distribution of its molecular Ca^{2+} sinks. Likewise, to our knowledge there is no report to date in any system which has systematically and quantitatively investigated the endogenous Ca^{2+} buffer distribution. Thus, we made an effort to shine some light on the quantitative distribution of the endogenous Ca^{2+} binding ratio as a determinant of local Ca^{2+} signals.

In this paper we present two complementary methods to study the endogenous Ca^{2+} buffer distribution: one aims at observing Ca^{2+} diffusion and the other avoids it. In both cases, we make the assumption that the reaction kinetics of the involved buffers is fast compared with the mean diffusional times, the so-called "rapid buffer approximation (rba)" (Wagner and Keizer, 1994). This is justified by virtue of recent studies (Naraghi, 1997; Xu et al., 1997) where the on- and off-rates for Ca^{2+} binding of some exogenous buffers as well as the endogenous buffer in adrenal chromaffin cells were investigated. There it was shown that the on-rate of the endogenous buffer is $\sim 10^8$ M s^{-1} and the off-rate 10^4 s^{-1}. This implies that the endogenous buffer reaches chemical equilibrium within <1 ms. Similarly, the exogenous buffers, which we used here, achieve equilibrium within <5 ms. Together, these justify the use of rba in our system.

In the first approach, we explore the extent to which the apparent Ca^{2+} diffusion is influenced, i.e., slowed by the presence of an immobile endogenous buffer using Eq. 3. Neher and Augustine (1992) have shown that there are no signs of Ca^{2+} release or uptake within 100 ms after a short depolarizing pulse. Thus, we explicitly aim at observing the dissipation of Ca^{2+} gradients from which we extract local Ca^{2+} diffusion coefficients. This approach can be characterized by the following criteria:

1. The source of the Ca^{2+} for inducing the gradients, and particularly its strength, is not a primarily relevant issue. The temporal spread of the Ca^{2+} signal and well-defined gradients of $[Ca^{2+}]$ throughout the cell are important. Our sources here are voltage-gated Ca^{2+} channels.
2. We should be aware of the influence of the Ca^{2+} indicator in shaping the gradients. It expresses itself in two quantities: the indicator's binding ratio κ_{ind} and its diffusion coefficient D_{ind}.
3. The deduction of diffusion coefficients, and thus binding ratios, from observations of Ca^{2+} diffusion is inverse to the classical simulation problem. There, knowing the parameters of the diffusion equation, one asks for the temporal evolution of its solution. Here, observing the

solution to the diffusion equation by imaging techniques, one asks for the parameters of the system. This corresponds to a nonlinear high-pass filtering of the Ca^{2+} images. Consequently, this process amplifies noise, which in turn imposes high requirements on the SNR of the imaging system.

4. For the applicability of the inverse method, it is essential to have moderate Ca^{2+} gradients such that the apparent Ca^{2+} diffusion coefficient in Eq. 3 can be regarded as independent of $[Ca^{2+}]$.
5. Ca^{2+} diffusion in the cell is an inherently 3-D problem, whereas given the temporal resolution of presently available imaging systems, one is only able to observe the Ca^{2+} signals in one focal slice. Then, one needs to simplify assumptions about the underlying cellular geometry. Here, we assume radial Ca^{2+} diffusion.
6. There are two possible sources for a locally reduced apparent Ca^{2+} diffusion coefficient: either a locally increased immobile Ca^{2+} binding ratio or deviations from the concept of diffusion in an isotropic medium, for instance because of local diffusion barriers. There is no direct way of distinguishing between these two possibilities.

Our diffusion measurements indicated local gradients of the apparent Ca^{2+} mobility at the boundary of the cell and at the nuclear envelope. One could attribute this to increased binding ratios close to biological membranes because of Ca^{2+} binding to membrane phospholipids or Ca^{2+} binding to specific buffers as an indication of functional organization of the cell, but this is only one possibility. These effects also may have been due to non-radial Ca^{2+} diffusion in 3-D and/or the nuclear envelope as a diffusion hindrance in conjunction with optical blurring effects. To separate these possibilities, we decided to apply flash photolysis of Ca^{2+}-loaded DMN as a light-dependent Ca^{2+} source (Kaplan and Ellis-Davies, 1988) together with Ca^{2+} imaging using Eq. 5. The flash photolysis technique was also used in a study by Al-Baldawi and Abercrombie (1995) together with Ca^{2+}-sensitive electrodes to measure the average Ca^{2+} binding ratio of the giant axon of the marine invertebrate Myxicola. The main characteristics of this approach can be summarized as 1) The strength of the source must be defined in order to extract the endogenous binding ratios from the comparison of preflash $[Ca^{2+}]$ with postflash $[Ca^{2+}]$. This requires careful calibration of the flash system in terms of its photolysis efficiency. 2) It is important to acquire the images as fast as possible to prevent inhomogeneities of the postflash $[Ca^{2+}]$ distribution to disappear by means of Ca^{2+} diffusion during the acquisition time of the image. 3) The indicator's diffusion coefficient, D_{ind}, effectively determines the spatial resolution by determining the mean diffusional path length of Ca^{2+} during an image acquisition. Its binding ratio, κ_{ind}, determines the fraction of the released Ca^{2+}, which is bound to the indicator. It should be of the same order of magnitude as κ_{endo}. 4) To attribute any heterogeneity of postflash $[Ca^{2+}]$ to the endogenous buffer distribution, it is critical to guarantee a spatially homogeneous photolysis efficiency.

With these constraints in mind, the performed photolysis experiments revealed no significant signs of heterogeneous buffer distribution. This attributes the slowing of Ca^{2+} diffusion near the nuclear membrane to its action as a diffusion barrier rather than to a high Ca^{2+} binding power. Furthermore, the near membrane D_{app} distribution must be interpreted as the result of deviations from radially symmetric diffusion in conjunction with blurring effects. Indeed, by looking at the Ca^{2+} independent fluorescence at different focal planes, the cell appears to be flat rather than spherical. We can conclude the photolysis experiments allow us to distinguish between different interpretations of the diffusion experiments and establish a more direct means of assessing the endogenous buffer distribution, but what is the spatial resolution of our measurement? Our pixel size (in the lateral direction) in the object plane is 580 nm. The effective resolution, nevertheless, is determined by the temporal resolution of the imaging system as well as the optical blurring effects in the axial direction. As mentioned earlier, we need 25 ms for the acquisition of an image.

Fig. 8 depicts the expected apparent Ca^{2+} diffusion coefficient and the mean displacement of Ca^{2+} ions (during this 25 ms) as a function of the exogenous binding ratio, assuming an endogenous ratio of 40 and a diffusion coefficient of 120 $\mu m^2/s$ for the dye. With an exogenous binding ratio of 50 to 100, we expect the mean Ca^{2+} displacement to be ~ 2 μm. Thus we have to restate our result in light of this temporal blurring: on a spatial grid with a lateral resolution of ~ 2 μm, there are no signs of heterogeneous buffer distribution in the bovine adrenal chromaffin cell. But there is also a spatial blurring because of the wide field imaging, which is applied in this paper. By using fluorescent beads as point sources of light, we experimentally measured the point spread function (PSF) of our optical system. From the measured PSF, we expect an axial resolution of 2–3 μm, which is of the same order of magnitude as the effective lateral resolution. In effect, we are dealing with cubic voxels with ~ 2 μm side length. To improve the spatial resolution, one would optimally need the axial resolution of a two-photon excitation system (reducing axial blurring) in conjunction with a significantly faster imaging system (reducing temporal blurring). For instance, to have a lateral resolution of $\sim$500 nm, we would need image acquisition times of ~ 2 ms, which is far beyond generally available technology and at the cutting edge of the mean reaction times of the high-affinity indicators (see Fig. 5). In addition, since we cannot afford an exogenous binding ratio much more than 100, there is an upper limit to the tolerable dye concentration. To get a meaningful fluorescence signal within 2-ms integration, the fluorescence yield of the Ca^{2+} indicators must be very high. Simultaneously, we must maintain our ability to measure $[Ca^{2+}]$, but there is no two-photon system up to date that allows measurement of $[Ca^{2+}]$ with such high rates. To conclude, imaging systems with 1) significantly higher acquisition rates, 2) the axial

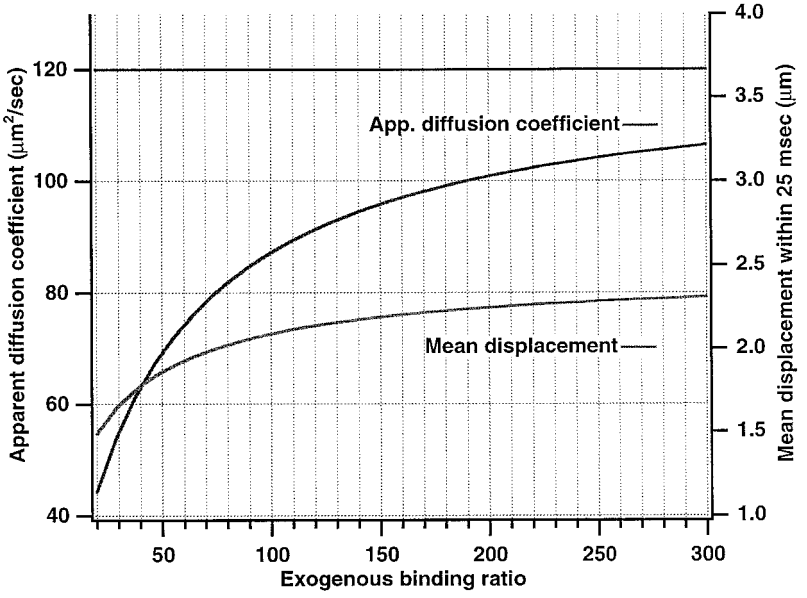

FIGURE 8 Dependence of the apparent Ca^{2+} diffusion coefficient on the exogenous binding ratio. We have plotted the apparent Ca^{2+} diffusion coefficient according to Eq. 9 as a function of the exogenous binding ratio, assuming an immobile buffer with a binding ratio of 40 and a dye of Bis-Fura-2 type with D_{ind} = 120 $\mu m^2/s$. Even at the concentration range where the exogenous buffer has similar binding ratios like the endogenous one (50–100), D_{app} is ~70–90 $\mu m^2/s$. Within the 25-ms frame integration time, this gives rise to a mean Ca^{2+} displacement of ~1.8–2.2 μm. Consequently, although the pixel size in the object plane is ~580 nm, the effective spatial resolution is ~2 μm and is dictated by the acquisition time for a frame.

resolution properties of a two-photon system, and 3) improved detector quantum yields in conjunction with much brighter Ca^{2+}-sensitive dyes, are necessary to improve the effective spatial resolution of the Ca^{2+} buffer measurements. Our resolution of 2 μm, of course, does not exclude buffer gradients on a finer spatial grid.

APPENDIX

$[Ca^{2+}]$ measurements

Conventional $[Ca^{2+}]$ measurements with ratiometric dyes involve excitation of the dye at two different wavelengths (Grynkiewicz et al., 1985). The fluorescence ratios are then used to calculate $[Ca^{2+}]$. Hence, the rate of $[Ca^{2+}]$ measurement is half the acquisition rate of the imaging system. In addition, there is an overhead due to the time needed to change the excitation wavelength, which is 2 ms in our system. To maximize the rate of $[Ca^{2+}]$ measurement, we implemented a modified dual wavelength excitation pattern which is based on the concept of the "isocoefficient" as described previously by Zhou and Neher (1993): let us assume that the fluorescent Ca^{2+} dye B is excited at two different wavelengths, λ_1 and λ_2, and the fluorescence in response to the two different excitation wavelengths, F_1 and F_2, is sampled. Then, F_i is given by

$$F_i = a_i I_i (f_{i,CaB}[CaB] + f_{i,B}[B] + b_i) + d, \qquad \text{(A1)}$$

where I_i is the excitation intensity, $f_{i,X}$ the specific fluorescence yield of the molecule X, b_i some coefficient representing the autofluorescence without dye loading, and a_i some gain factor, all at wavelength λ_i. Furthermore, d is the dark current offset. Using the above-mentioned photodiode, we monitor the excitation intensities likewise as $R_i = I_i g_i$, with g_i being some proportionality factor. We measure the offset d and the autofluorescence $a_i I_i b_i$ of the cell before dye loading, subtract this background, and divide this signal by the excitation intensities R_i to obtain the normalized quantities

$$F_i' = \frac{F_i - d - a_i I_i b_i}{R_i} = \frac{a_i}{g_i}(f_{i,CaB}[CaB] + f_{i,B}[B]). \qquad \text{(A2)}$$

Both signals F_i' are Ca^{2+}-sensitive. Nevertheless, a constant α (the so-called isocoefficient) can be found, which makes the linear combination $F_2'' = F_2' + \alpha F_1'$ independent of the free Ca^{2+} concentration, as long as the diffusion coefficient of the dye is not changed by binding a Ca^{2+} ion. It is easy to show that α is given by

$$\alpha = \frac{-a_2 g_1}{a_1 g_2}\frac{f_{2,CaB} - f_{2,B}}{f_{1,CaB} - f_{1,B}} \equiv \frac{-a_2 g_1}{a_1 g_2}\alpha_0,$$

i.e., by dye and instrumentation parameters. We determined α experimentally by depolarizing the cells for 25–100 ms to 0 mV (or by photoreleasing Ca^{2+} from DMN loaded in the cell) in the whole-cell mode to increase $[Ca^{2+}]$, acquiring the fluorescence images F_1 and F_2 for λ_1 = 385 nm and λ_2 = 350 nm at rest as well as after increasing $[Ca^{2+}]$ and calculating the normalized images F_1' and F_2' for both $[Ca^{2+}]$ levels. Then we applied the Levenberg-Marquardt least-squares algorithm (Press et al., 1992) to find a scalar quantity α, which minimized the difference

$$\Delta = \sum_{k,l}[F_{2,2}'(k,l) + \alpha F_{1,2}'(k,l) - F_{2,1}'(k,l) - \alpha F_{1,1}'(k,l)]^2 \qquad \text{(A3)}$$

where the sum extends over all image pixels with coordinates (k, l) and $F_{i,j}'$ is the normalized fluorescence at excitation wavelength λ_i and $[Ca^{2+}]$ level j (j = 1 stands for resting $[Ca^{2+}]$ and j = 2 for elevated $[Ca^{2+}]$). This procedure resulted in an isocoefficient α for Fura-2 of 0.12 and 0.28 for Bis-Fura-2, respectively. To achieve fast $[Ca^{2+}]$ measurements, we calculated F_2'' as a Ca^{2+}-independent signal, applied a depolarizing pulse or a UV flash to raise $[Ca^{2+}]$, switched the wavelength to λ_1 = 385 nm, and acquired up to 10 consecutive images on the frame transfer chip with a frequency of 40 Hz (25 ms/image). Hence, for the 40 Hz acquisition rate, we only had single excitation wavelength images at our disposal. We then made the ratios $r = F_2''/F_1'$ of the Ca^{2+}-independent image over the Ca^{2+}-sensitive images. This results in

$$r = \frac{a_2 g_1}{a_1 g_2}\frac{\frac{[Ca^{2+}]}{K_D}(f_{2,CaB} - \alpha_0 f_{1,CaB}) + (f_{2,B} - \alpha_0 f_{1,B})}{f_{1,CaB}\frac{[Ca^{2+}]}{K_D} + f_{1,B}}. \qquad \text{(A4)}$$

In the limit of $[Ca^{2+}] = 0$ nM, we get $r_{min} = (a_2 g_1/a_1 g_2)$ $(f_{2,B} - \alpha_0 f_{1,B})/f_{1,B}$, and for very high $[Ca^{2+}]$ levels, we obtain $r_{max} = (a_2 g_1/a_1 g_2)$ $(f_{2,CaB} - \alpha_0 f_{1,CaB})/f_{1,CaB}$. Using these identities, Eq. A4 can be rewritten as

$$[Ca^{2+}] = K_D \frac{f_{1,B}}{f_{1,CaB}} \frac{r - r_{min}}{r_{max} - r} \equiv K_{eff} \frac{r - r_{min}}{r_{max} - r}, \quad \text{(A5)}$$

which is a Grynkiewicz-type formalism. Consequently, we determined r_{min} and r_{max} according to the in vivo procedure of Neher (1989) by dialyzing cells with internal solutions containing either 10 mM BAPTA or 10 mM $CaCl_2$ and calculating the ratios according to the above definition. For K_{eff}, 10 mM BAPTA and 5 mM $CaCl_2$ were added to the internal solution to give $[Ca^{2+}] = 225$ nM (Zhou and Neher, 1993). The ratio images were converted into $[Ca^{2+}]$ images with continuous 40 Hz acquisition at the Ca^{2+}-dependent wavelength (385 nm) using a Ca^{2+}-independent reference image based on the isocoefficient formalism. The Ca^{2+}-independent image was assumed to be time-independent.

Calibration of the photolysis efficiency of the flash lamp

In the photolysis experiments, it was crucial to know the total amount of Ca^{2+} that was liberated into the cytosol after photolytic cleavage of Ca^{2+}-loaded DMN. In addition, by adjusting the discharge voltage of the lamp, one could manipulate the intensity of the flash and, thus, the fraction of DMN that was cleaved. The photolysis efficiency inside the cell was determined in the following manner: we patched chromaffin cells in whole-cell mode using internal solutions that contained 1 mM Bis-Fura-2 and 1 mM fully Ca^{2+}-loaded DMN, in the absence of magnesium. We measured $[Ca^{2+}]$ before and after 200–300 V discharges of the flash lamp, with different neutral density filters (OD = 0.5–1.3) inserted into the light path to attenuate the flash. Since the released Ca^{2+} can only bind to Bis-Fura-2 (which outcompetes the endogenous Ca^{2+} buffer) or appear as free Ca^{2+}, we arrive at the following conservation rule (P_e = photolysis efficiency):

$$P_e[DMN]_{total} = (\kappa_{Bis\text{-}Fura\text{-}2} + 1)\Delta[Ca^{2+}], \quad \text{(A6)}$$

where $\kappa_{Bis\text{-}Fura\text{-}2}$ is the Ca^{2+} binding ratio of Bis-Fura-2 (Neher and Augustine, 1992) and Δ indicates the difference before and after flash. With this procedure, we identified the efficiency of a 300 V discharge with an OD = 1.0 filter in the light path for cleaving CaDMN to be 5.6%. Furthermore, we checked that the calibration parameters of the dye (in the presence of 1 mM DMN) were not significantly altered after such a flash: r_{min} changed from 0.754 to 0.765, r_{max} from 8.235 to 8.167, and K_{eff} from 3296 to 3403 nM. In all photolysis experiments we used small photolysis efficiencies (2–7%) to prevent significant changes in calibration parameters.

Our work was stimulated by numerous discussions with the late Frederic S. Fay, whom we gratefully acknowledge. We also thank Frauke Friedlein and Michael Pilot for expert technical assistance, particularly for preparing chromaffin cells.

This work was supported by a grant from the Behrens-Weise-Stiftung (to E.N.).

REFERENCES

Al-Baldawi, N. F., and R. F. Abercrombie. 1995. Cytoplasmic calcium buffer capacity determined with Nitr-5 and DM-nitrophen. *Cell Calcium.* 17:409–421.

Allbritton, N. L., T. Meyer, and L. Stryer. 1992. Range of messenger action of calcium ion and inositol 1,4,5-trisphosphate. *Science.* 258: 1812–1815.

Chad, J. E., and R. Eckert. 1984. Calcium "domains" associated with individual channels may account for anomalous voltage relations of calcium-dependent responses. *Biophys. J.* 45:993–999.

Clapham, D. E. 1995. Calcium signaling. *Cell.* 80:259–268.

Ellis-Davies, G. C. R., J. H. Kaplan, and R. J. Barsotti. 1996. Laser photolysis of caged calcium: rates of calcium release by nitrophenyl-EGTA and DM-nitrophen. *Biophys. J.* 70:1006–1016.

Grynkiewicz, G., M. Poenie, and R. Y. Tsien. 1985. A new generation of Ca^{2+} indicators with greatly improved fluorescence properties. *J. Biol. Chem.* 260:3440–3450.

Heinemann, C., R. H. Chow, E. Neher, and R. S. Zucker. 1994. Kinetics of the secretory response in bovine chromaffin cells following flash photolysis of caged Ca^{2+}. *Biophys. J.* 67:2546–2557.

Huser, J., S. L. Lipsius, and L. A. Blatter. 1996. Calcium gradients during excitation-contraction coupling in cat atrial myocytes. *J. Physiol.* 494: 641–651.

Imredy, J. P., and D. T. Yue. 1992. Submicroscopic Ca^{2+} diffusion mediates inhibitory coupling between individual Ca^{2+} channels. *Neuron.* 9:197–207.

Kaplan, J. H., and G. C. R. Ellis-Davies, 1988. Photolabile chelators for rapid photolytic release of divalent cations. *Proc. Natl. Acad. Sci. USA.* 85:6571–6575.

Kasai, H., and G. J. Augustine. 1990. Cytosolic calcium gradients triggering unidirectional fluid secretion from exocrine pancreas. *Nature.* 348: 735–738.

Llinas, R., M. Sugimori, and R. B. Silver. 1995. The concept of calcium concentration microdomains in synaptic transmission. *Neuropharmacology.* 34:1443–1451.

Louis, A. K. 1989. Inverse und schlecht gestellte Probleme. B. G. Teubner, Stuttgart.

Markram, H., and B. Sakmann. 1994. Calcium transients in dendrites of neocortical neurons evoked by single subthreshold excitatory postsynaptic potentials via low-voltage activated calcium channels. *Proc. Natl. Acad. Sci. USA.* 91:5207–5211.

Mathias, R. T., I. S. Cohen, and C. Oliva. 1990. Limitations of the whole-cell patch clamp technique in the control of intracellular concentrations. *Biophys. J.* 58:759–770.

Naraghi, M. 1997. T-jump study of calcium binding kinetics of calcium chelators. *Cell Calcium.* 22:255–268.

Neher, E. 1989. Combined fura-2 and patch clamp measurements in rat peritoneal mast cells. *In* Neuromuscular Junction. L. C. Sellin, R. Libelius, and S. Thesleff, editors. Elsevier Science, New York, 65–76.

Neher, E. 1995. The use of fura-2 for estimating Ca^{2+} buffers and Ca^{2+} fluxes. *Neuropharmacology.* 34:1423–1442.

Neher, E., and G. J. Augustine. 1992. Calcium gradients and buffers in bovine chromaffin cells. *J. Physiol. (Lond.).* 450:273–301.

O'Sullivan, A. J., T. R. Cheek, R. B. Moreton, M. J. Berridge, and R. D. Burgoyne. 1989. Localization and heterogeneity of agonist-induced changes in cytosolic calcium concentration in single bovine adrenal chromaffin cells from video imaging of Fura-2. *EMBO J.* 8:401–412.

Press, W. H., S. A. Teukolsky, W. T. Vetterling, and B. P. Flannery. 1992. Numerical Recipes in C. Cambridge University Press, Cambridge.

Smith, C., and E. Neher. 1997. Multiple forms of endocytosis in bovine adrenal chromaffin cells. *J. Cell Biol.* 139:885–894.

Tarantola, A. 1987. Inverse Problem Theory. Elsevier Science, Amsterdam.

Wagner, J., and J. Keizer. 1994. Effects of rapid buffers on Ca^{2+} diffusion and Ca^{2+} oscillations. *Biophys. J.* 67:447–456.

Williams, D. A., K. E. Fogarty, R. Y. Tsien, and F. S. Fay. 1985. Calcium gradients in single smooth muscle cells revealed by the digital imaging microscope using Fura-2. *Nature.* 318:558–561.

Xu, T., M. Naraghi, H. Kang, and E. Neher. 1997. Kinetic studies of Ca^{2+} binding and Ca^{2+} clearance in the cytosol of adrenal chromaffin cells. *Biophys. J.* 73:532–545.

Zhou, Z., and E. Neher. 1993. Mobile and immobile calcium buffers in bovine adrenal chromaffin cells. *J. Physiol. (Lond.).* 469:245–273.

Zucker, R. S. 1993. The calcium concentration clamp: spikes and reversible pulses using the photolabile chelator DM-nitrophen. *Cell Calcium.* 4:87–100.